Journal of Magnetism and Magnetic Materials 393 (2015) 99–104

Contents lists available at ScienceDirect

Journal of Magnetism and Magnetic Materials

journal homepage: www.elsevier.com/locate/jmmm

Influence of reverted austenite on the texture and magnetic properties of 350 maraging steel

Hamilton F.G. Abreu [a,1], Jean J. Silva [a,1], Manoel R. Silva [b], Marcelo J. Gomes da Silva [a,*]

[a] Universidade Federal do Ceará, Campus do Pici-Bloco 729, CEP 60440-554 Fortaleza, CE, Brazil
[b] Universidade Federal de Itajubá, Campus Sede Itajubá/IFQ- Instituto de Física e Química, Itajubá, MG, Brazil

ARTICLE INFO

Article history:
Received 19 April 2014
Received in revised form
12 May 2015
Accepted 16 May 2015
Available online 19 May 2015

Keywords:
Maraging steel
Reverted austenite
Texture
Martensite

ABSTRACT

The aging temperature to improve magnetic properties in Maraging-350 steel (Mar-350) is limited by the onset of austenite reversion. The traditional process of cooling after aging is to remove the piece from the oven and then to air cool it. The purpose of this research was to characterize the reverted austenite and to investigate the effect of cooling below the martensite start temperature (M_s) on the magnetic properties. The Mar350 samples aged at temperatures above 550 °C, and subsequently cooled in liquid nitrogen presented less austenite than samples cooled in air, resulting in higher magnetization saturation and a lower coercive force. A combination of optical microscopy (OM), X-ray diffraction (XRD) and electron backscatter diffraction (EBSD) techniques were used to characterize the presence of reverted austenite. The crystallographic texture of both martensite and reverted austenite were analyzed. The texture of the reverted austenite coincides with the texture of the parent austenite indicating that a phenomenon of texture memory is present.

1. Introduction

Maraging steels are a family of iron-based metallic materials that combine extremely high mechanical strength and good toughness. This family of steels has important applications in the production of magnets for high speed rotors, in which the limiting condition is the yield strength of the materials used, thus constituting the main barrier for further development and utilization of materials for such applications. Most of the magnetic materials used do not combine the desirable mechanical and magnetic properties [1,2]. The aging temperature that results in the best mechanical properties differs from the one that confers the best magnetic properties. The highest yield stress levels are achieved after aging for 1 h at 480 °C, in which the precipitation of intermetallic compounds such as Ni_3Ti, Ni_3Mo, Fe_2Mo and Fe_7Mo_6 acts as the hardening mechanism [3]. To improve the magnetic properties, the aging temperature should be higher than 480 °C but is limited by the onset of austenite reversion. Austenite formation occurs between 500 °C and 700 °C and promotes an increase in the coercive force and a decrease in the magnetization saturation. The austenite phase is a result of the dissolution of precipitates that form in Ni rich regions. The high Ni concentration in some regions decreases the martensite start (M_s) temperature to negative values [4,5]. Two types of reverted austenite morphology are reported in the literature: one that forms at the boundary of lath martensite and another that grows inside the lath martensite [6].

In a previous paper, the A_s, A_f, M_s, and M_f temperatures were measured for 80% cold-rolled Mar350 using thermomagnetic analysis. The temperatures were found to be 690 °C, 800 °C, 175 °C, and 130 °C, respectively [7]. These temperatures change with the degree of deformation before aging [7–9]. In a previous work [7], quantifications of the austenitic phase of a Mar300 steel, which was heat treated at different temperatures and for different periods of time, were undertaken using the direct comparison method by X-ray diffraction (XRD). The results showed an increase in austenite content for aging times associated with 560 °C and 600 °C; however, in the samples aged at 650 °C, the austenite content decreased and the martensite parameter increased with aging times above 1 h [10].

The present work examined the influence of the cooling rate on the phase fraction of the reverted austenite and how the mechanical properties (addressed via hardness measurements), coercive force and magnetization saturation were affected. The characterization of the reverted austenite, crystallographic texture, orientation relationship with martensite and the applicability of the phenomenological martensite transformation crystallography (PMTC) were also discussed [11–16].

* Corresponding author. Fax: +55 85 3366 9969.
E-mail addresses: hamilton@ufc.br (H.F.G. Abreu), mgsilva@ufc.br (M.J. Gomes da Silva).
[1] Fax: +55 85 3366 9969.

http://dx.doi.org/10.1016/j.jmmm.2015.05.037
0304-8853/

2. Experimental

Cold-rolled Mar350 steel samples containing 19.77 Ni, 10.74 Co, 4.70 Mo, 1.4 Ti, 0.10 Al, 0.0073 C (wt%) and the balance Fe, were solution annealed at 870 °C for 1 h and then air cooled. In sequence, the samples were aged at temperatures ranging from 450 °C to 650 °C for 1 h. XRD experiments were conducted in a Panalytical X'Pert Pro diffractometer using Co-Kα radiation with an attached monochromator. Orientation distribution functions (ODF) were calculated for incomplete pole figures-(110), (200), and (211) for martensite and (200) and (220) for austenite-with a maximum tilt of 75°. The ODF was calculated for these poles using the ADC method from LABOTEX texture software. The magnetic properties were determined using a vibrating sample magnetometer. A maximum field of 10,000 Oe was applied during the measurements. Hardness was measured in a Shimadzu microhardness tester using an applied load of 0.1 kg f for 30 s. Electron backscatter diffraction (EBSD) maps were obtained using an FEI XL-30 SEM equipped with an Oxford-HKL EBSD system. HKL-Oxford Channel 5 software was used for the EBSD analysis.

The sample preparation for the EBSD experiments followed the classical sequence of mechanical grinding with silicon carbide paper (120–1200 grit sequence), followed by mechanical polishing down to a 0.05 μm diamond. Finally, in order to achieve the high degree of polishing necessary for good quality Kikuchi diffraction patterns, 6–8 h of colloidal silica polishing were undertaken.

3. Results and discussion

3.1. The effect of cooling rate on austenite reversion

Aging treatments above 550 °C promote the reversion of austenite in maraging steels. The phase fraction of the formed austenite can be totally or partially retained at room temperature after cooling, depending on the chemical composition. Nickel content plays a major role in the stability of the austenitic phase as a result of the dissolution of precipitates formed in Ni rich regions. The reversion of austenite results in a γ′phase richer in Ni and an α_2' phase poorer in Ni [5]. The composition variation of the austenite phase with temperature was calculated with Thermocalc software as shown in Table 1 as well as calculated M_s temperatures according to two different references [17,18].

The calculated content of Ni is compatible with the measured values obtained by Ahmed et al. [3]. According to the calculations, the Ni content necessary to stabilize austenite decreases with an increase in temperature, reaching the nominal composition of the alloy at 700 °C. The calculated compositions were used to estimate the M_s temperatures (last two columns of Table 1), by employing the empirical formula shown in Equation 1 [17] and Equation 2 [18]. Note that both references use a greater set of alloying elements than the ones actually present on the current alloy. Both are general and are meant to include all variations of alloy compositions. The formula proposed in Eq. (1) is a more general steels and the later proposed in Eq. (2) is a more specific for maraging grade alloys. The M_s temperature of maraging steels must be closely controlled in order to ensure complete transformation of austenite to martensite. Because M_s is mainly a function of alloy chemistry, the usual requirement for the composition throughout the development of maraging steels is to guarantee an M_s above room temperature. Most of the data available for M_s modeling is for alloys with more that four components, however the expressions are not fully tested for multiple component alloys since the majority of the data is for ternary or quaternary alloys [18].

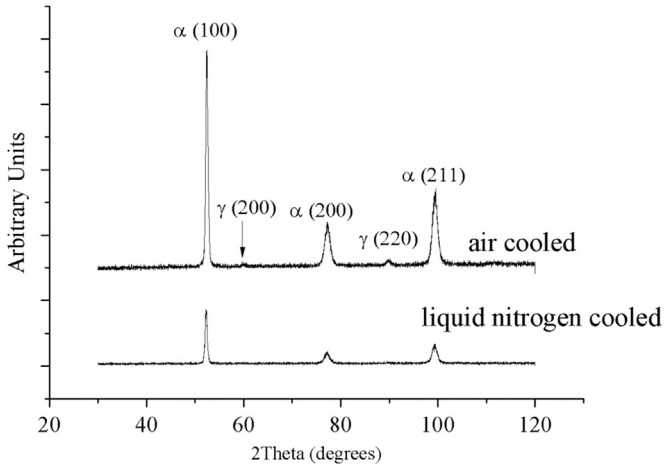

Fig. 1. XRD patterns of the sample aged at 550 °C for 1 h followed by air and liquid nitrogen cooling.

$$M_s(°C) = 539 - 433\,C - 30.4Mn - 12.1Cr - 17.7Ni - 7.5Mo \quad (1)$$

$$M_s(°C) = 549 - 500\,C + 15.9Al - 3.8Co - 18.3Cr - 6Cu - 22Mn + 0.2Mo - 1.6Nb - 17.5Ni - 10Si - 29Ti - 54V \quad (2)$$

For the aging temperature of 550 °C, the calculated M_s temperature falls below −40 °C, which means that, with cooling in liquid nitrogen after 1 h aging, there is no stable reverted austenite at room temperature. Fig. 1 compares the XRD patterns for samples aged for 1 h at 550 °C followed by air and liquid nitrogen cooling. The sample cooled in air showed peaks of austenite different from the sample cooled in liquid nitrogen where only martensite peaks are present.

Fig. 2 compares the phase volume fraction of reverted austenite for the 90% cold-rolled samples aged at 450 °C to 650 °C and cooled in air and liquid nitrogen. For samples aged at temperatures above 550 °C, a lower phase fraction of reverted austenite is observed when the sample is cooled in liquid nitrogen as compared to air. In a similar experiment, Ahmed reported a decrease of 4% in the phase fraction of reverted austenite when the sample was cooled in liquid nitrogen. An explanation for this is that both the M_s and M_f (the temperature at which the martensite formation associated with cooling is finished) are being reached. The quantification of the reverted austenite was undertaken using the direct comparison method—a more detailed explanation of these calculations can be found in Ref. [10].

The presence of reverted austenite changes both the magnetic and mechanical properties. Fig. 3 compares the saturation

Table 1
Calculated composition of reverted austenite at different aging temperatures.

	Fe (wt%)	Co (wt%)	Ti (wt%)	Ni (wt%)	Mo (wt%)	M_s temperature (°C) [17]	M_s temperature (°C) [18]
550 °C	59.0	5.6	0.25	**31.4**	3.5	−43	−28.3
600 °C	62.0	7.5	0.5	**25.7**	4.3	52	57.1
650 °C	63.3	10.0	1.0	**20.6**	4.8	138	122.5
700 °C	63.4	10.7	1.4	**19.7**	4.8	154	124

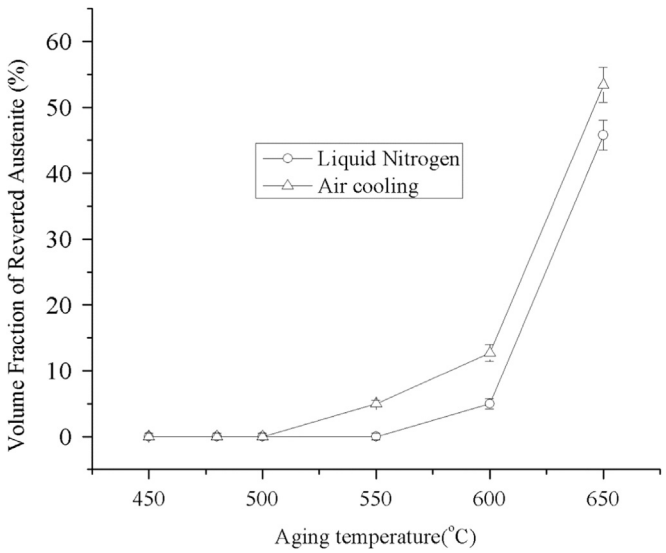

Fig. 2. Quantification of the austenitic phase by XRD for samples cold rolled to 90% thickness, aged for 1 h and cooled in air and liquid nitrogen.

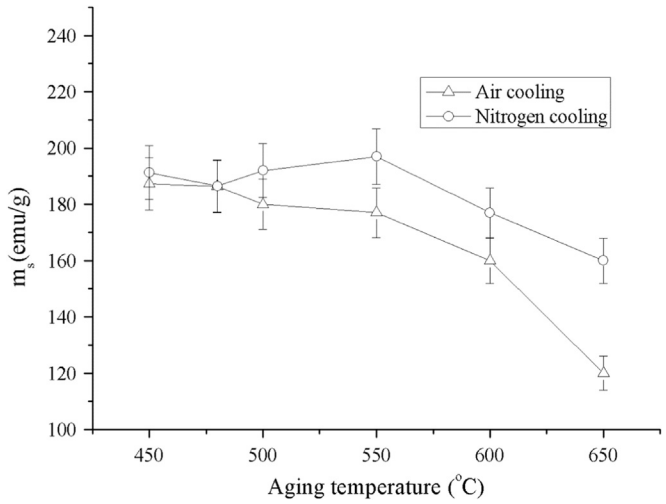

Fig. 3. Magnetization saturation for samples cooled in air and liquid nitrogen.

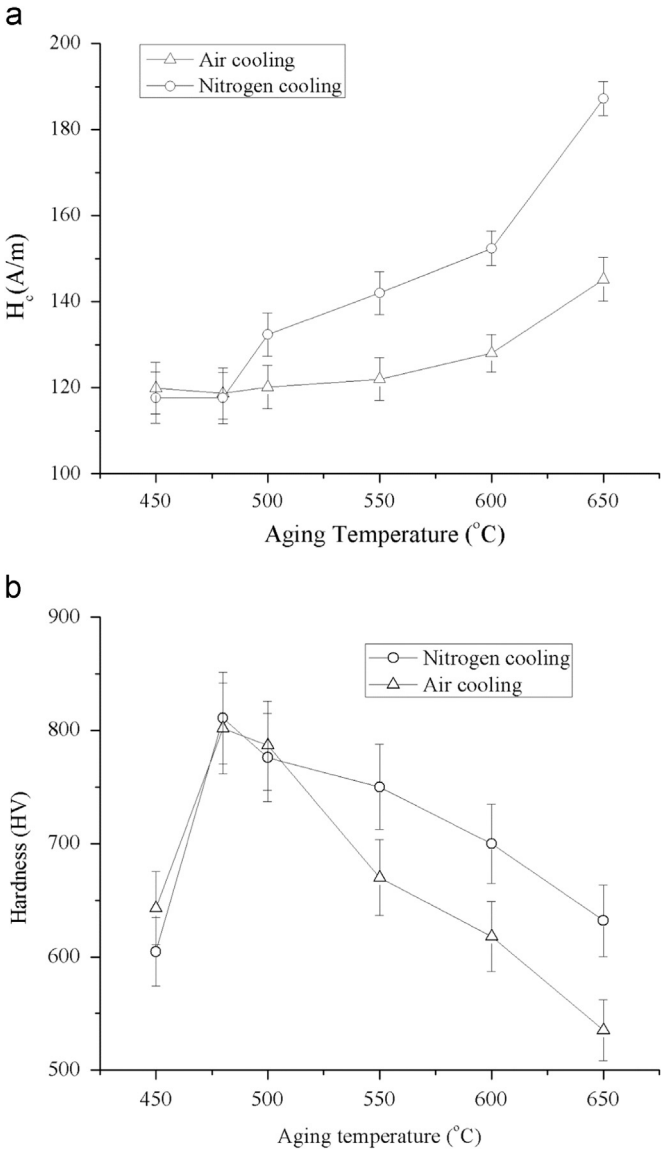

Fig. 4. (a) Coercive force and (b) hardness for samples cooled in air and liquid nitrogen.

magnetization (m_s) for samples aged at 450 °C, 500 °C, 550 °C, 600 °C, and 650 °C. The saturation magnetization decreases with increasing aging temperatures. This effect is more pronounced in samples cooled in air where the fraction of reverted austenite is higher. The coercive force (H_c) and hardness (H_V) are also affected by the fraction of reverted austenite. Cooling in liquid nitrogen resulted in smaller H_c values as seen in Fig. 4(a). Samples cooled in liquid nitrogen had a smaller decrease in hardness with increasing aging temperature when compared with samples cooled in air (Fig. 4(b)). The presence of a smaller austenite fraction, a softer phase, resulted in a hardness gain for the nitrogen cooled samples.

3.2. Characterization of reverted austenite

The characterization of austenite was taken in samples cooled in air due to the greater amount of this phase when using this cooling medium, as was shown in the previous section. Fig. 5 shows an optical micrograph of a sample solution annealed for 1 h at 870 °C, air cooled, aged for 1 h at 550 °C and then air cooled. The sample was etched with modified picral to reveal the retained austenite [19]. The white regions in Fig. 5 are austenite precipitated on the boundaries of the martensite plates. Two types of

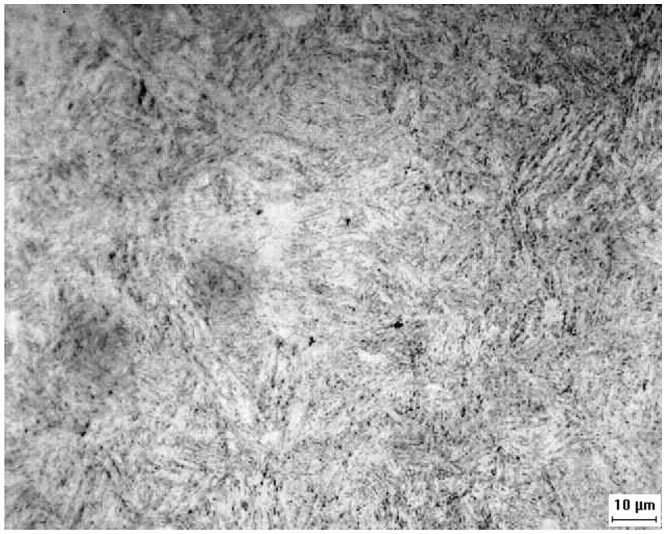

Fig. 5. Optical micrograph for a sample aged at 550 °C and air cooled. (Magnification: 1000 ×; Etchant: modified picral).

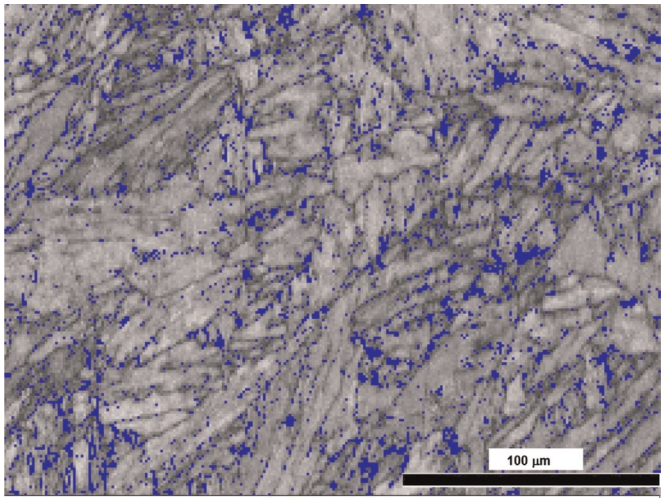

Fig. 6. EBSD quality map showing reverted austenite for a solution-annealed 90% cold-rolled sample aged at 600 °C for 1 h.

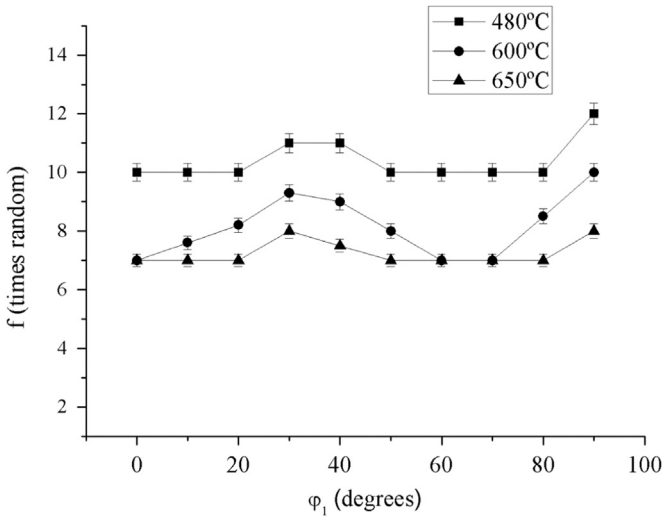

Fig. 8. Intensity of ODF for γ-fiber at $\varphi_2=45°$ in 90% cold-rolled samples, aged at 480 °C, 600 °C and 650 °C, followed by air cooling.

reverted austenite morphologies have been reported in the literature. The first is the inter-lath austenite which nucleates at the martensite lath boundaries; the second is known as intra-lath reverted austenite, which grows inside the martensite laths in the form of twins [8]. Fig. 6 shows a quality EBSD map for a sample aged for 1 h at 600 °C and air cooled. The blue color phase along the martensite laths is reverted austenite. It is clear that reverted austenite has precipitated at the boundary of the martensite lathes, therefore confirming that its formation follows the first mode described in the previous paragraph.

Another aspect of the presence of reverted austenite is the change in the crystallographic texture of martensite. Fig. 7 shows sections of $\varphi_2=45°$ of ODF for samples aged at 480 °C, 600 °C, and 650 °C, and then cooled in air. As seen in Fig. 2, the sample aged at 480 °C did not present any reverted austenite. Samples aged at 600 °C and 650 °C presented 12.7 and 53.4 wt% of reverted austenite, respectively. The change in the crystallographic texture is the reduction of the intensity of the γ-fiber ($<111>$//normal direction). This fiber is represented at $\varphi_2=45°$ by a line at $\phi=45°$. Fig. 8 shows the reduction in intensity of this fiber with increasing temperatures in 10° intervals with an error of 3%. It is possible that martensite with $\{111\}<uvw>$ orientations is more susceptible to transform back to austenite. The texture of reverted austenite was measured for the sample aged at 650 °C and cooled in air, which presented the greatest fraction of reverted austenite among all the samples examined.

The ODF section of $\varphi_2=45°$ for the reverted austenite is shown in Fig. 9. The texture is characterized by the presence of two intense components, goss and copper, which is characteristic of face centered cubic (FCC) materials like austenitic stainless steels. This result strongly suggests that the orientation of the reverted austenite follows the same orientation as the previous, pre-aging, austenite (after solution annealing and prior to the martensitic transformation upon cooling). Confirmation of this was obtained by comparing EBSD results with the expected orientations calculated with the PMTC [14–16].

An EBSD study was undertaken to compare the texture of the reverted austenite with the texture of the parent austenite. The texture of a central grain in Fig. 10 was used as an input to calculate the transformation texture of the martensite. The calculated pole figures based on the phenomenological theory of martensite (PMTC) were compared with measured EBSD pole figures [12].

Selecting the central region in Fig. 10(b), where the reverted austenite is more closely populated, the set of Euler angles, $\varphi_1=334.3°$, $\phi=47.9°$, and $\varphi_2=60.3°$, representing the orientation of austenite which corresponds to the orientation matrix in Eq. (3), is obtained directly from the EBSD map. The matrix representation is more suitable for texture transformation calculations

$$(S\,J\,\gamma)=\begin{pmatrix}0.69899 & 0.30989 & 0.6445\\ -0.63866 & 0.67600 & 0.36672\\ -0.32176 & -0.66858 & 0.67043\end{pmatrix} \quad (3)$$

To perform such a calculation, a complete set of crystallographic data is necessary. Unfortunately, such data for maraging steels was not available. Instead, a data set that corresponds to the

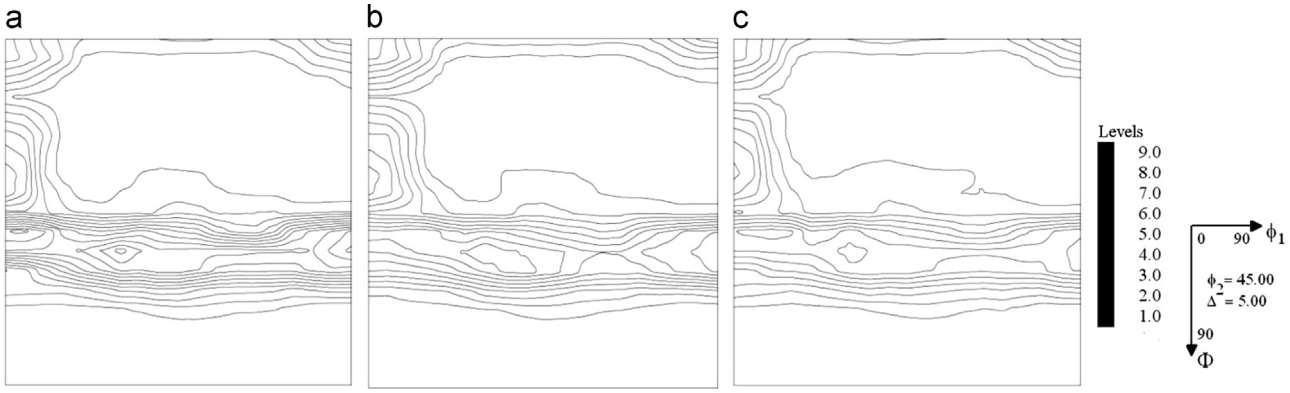

Fig. 7. ODFs for 90% cold-rolled samples aged at (a) 480 °C, (b) 600 °C, and (c) 650 °C, followed by air cooling.

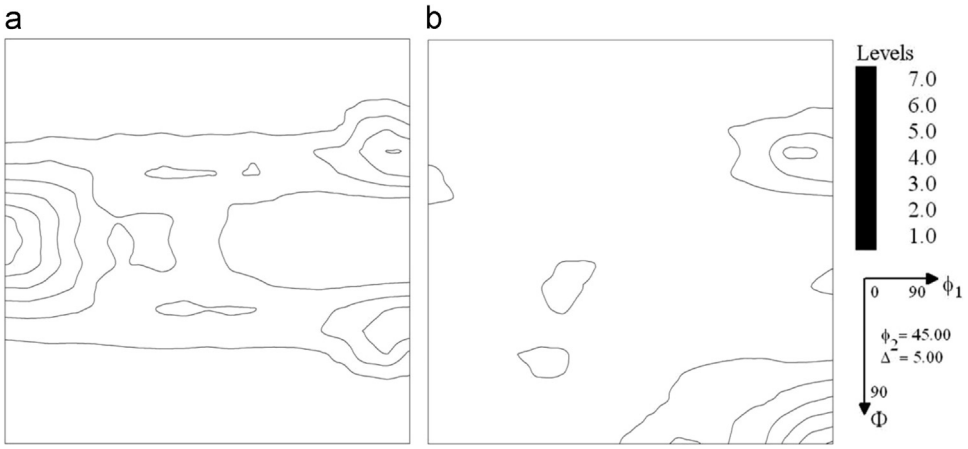

Fig. 9. ODF sections (a) $\varphi_2=0°$ and (b) $\varphi_2=45°$ for the reverted austenite in 90% cold-rolled samples aged at 650 °C and air cooled.

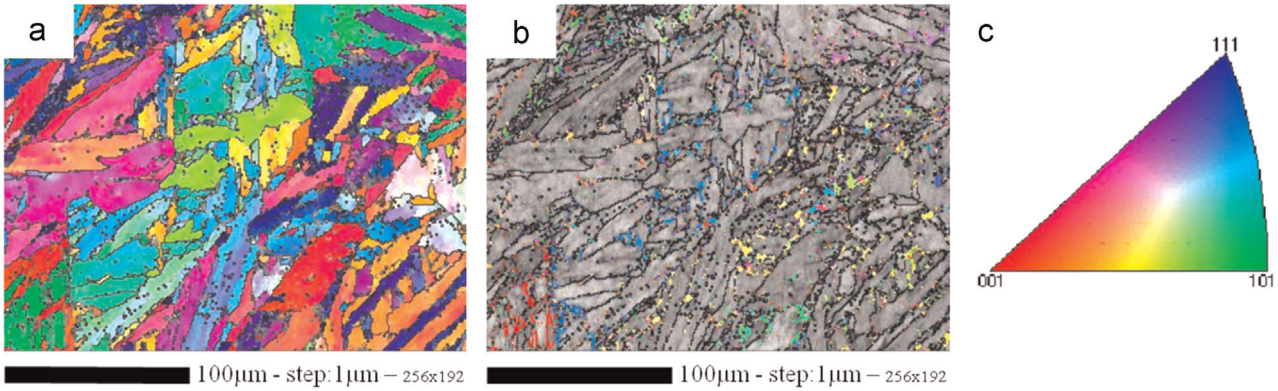

Fig. 10. (a) EBSD orientation image for martensite; (b) orientation imaging maps of martensite (gray lathes) and reverted austenite (colored inter-lathes); (c) color key for crystallographic orientations. (For interpretation of the references to color in this figure legend, the reader is referred to the web version of this article.)

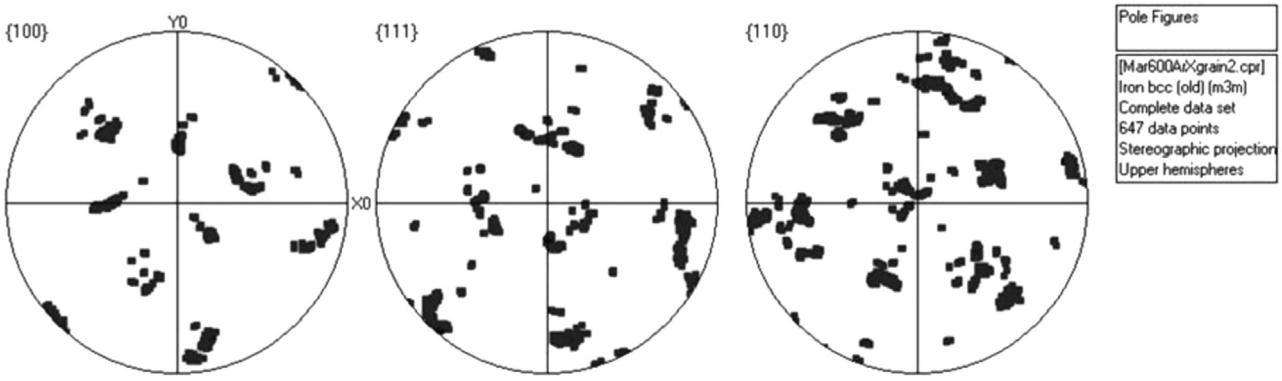

Fig. 11. Martensite calculated (100), (110), and (111) pole figures, assuming the presence of all 24 variants.

traditional twinning $\{259\}_\gamma$ transformation found in Fe–Ni and Fe–Ni–C, was utilized [19,20] as maraging alloys come primarily from FeNi systems. Working with this set we found the orientation matrix (γ J α) in Eq. (4)

$$(\gamma\ J\ \alpha) = \begin{pmatrix} 0.577230 & 0.542366 & 0.099860 \\ -0.551364 & 0.570563 & 0.088221 \\ -0.011434 & -0.132757 & 0.787130 \end{pmatrix} \quad (4)$$

Multiplying the orientation matrix (S J γ) by the transformation matrix (γ J α) the orientation matrix of martensite (S J α) is obtained. Multiplying (S J α) by the set of symmetry matrices we obtain all 24 of the possible variants. Fig. 11 shows the calculated (100), (110) and (111) martensite pole figures, assuming that all 24 variants are present. These pole figures should be compared with the measured pole figures presented in Fig. 12.

The calculated martensite pole figures from the measured reverted austenite (set of Euler angles) are in close agreement with the measured martensite pole figures from the mother austenite phase. There is a very good match between the calculated and the measured pole figures, indicating that the reverted austenite and parent phase show the same crystallographic texture as the orientation of the martensite match. Also, such an agreement indicates the occurrence of the texture memory effect phenomenon, where reverted austenite recovers the mother phase's original texture.

Confirmation of this statement was achieved by simulating the inverse transformation. The set of Euler angles for 3 different

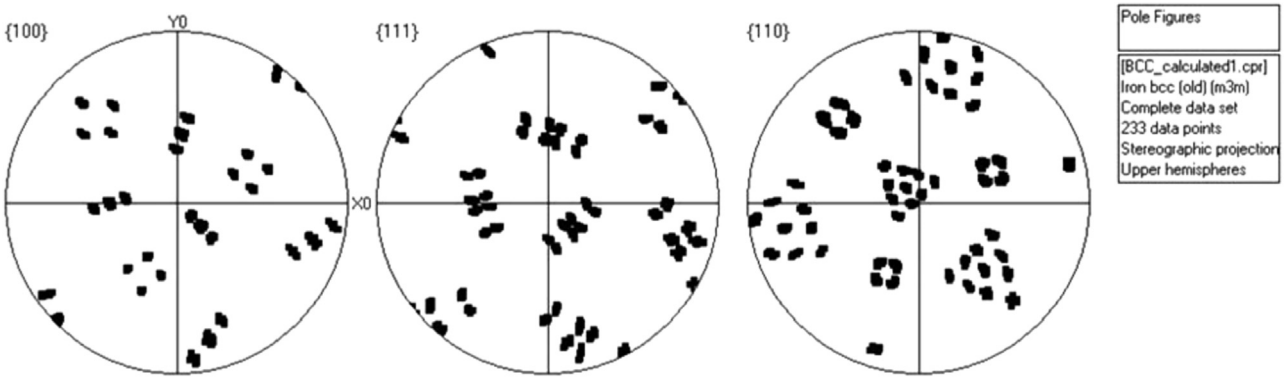

Fig. 12. Martensite EBSD measured (100), (110), and (111) pole figures.

martensite laths close to the measured reverted austenite was determined by EBSD. They were respectively lath 1 ($\varphi_1=46.2°$, $\phi=29.2°$, and $\varphi_2=88.6°$); lath 2 ($\varphi_1=175.7°$, $\phi=42.7°$, and $\varphi_2=82.7°$); and lath 3 ($\varphi_1=121.0°$, $\phi=41.1°$, and $\varphi_2=70.0°$). They generate three orientation matrices (SJα). Multiplying each (SJα) by Eq. (5), the matrix (αJγ), and then multiplying by the set of 24 symmetry matrices, 24 possible austenite orientations were determined for each martensite orientation. In each of the three groups of 24 possible orientations the set of Euler angles $\varphi_1=334.3°$; $\phi=47.9°$; and $\varphi_2=$ 60.3 º were present.

$$(\alpha J\gamma) = \begin{pmatrix} 0.905785 & -0.865046 & -0.017298 \\ 0.850916 & 0.895168 & -0.208965 \\ 0.156672 & 0.138412 & 1.234942 \end{pmatrix} \quad (5)$$

4. Conclusions

The main conclusions resulting from this work are:

The Ni content necessary to stabilize austenite decreases with an increase in aging temperature, thus affecting the M_s temperature, and consequently, the phase fraction of reverted austenite when a sample is aged and cooled in liquid nitrogen.

Cooling samples in liquid nitrogen after aging above 550 ºC reduces the phase fraction of reverted austenite and increases magnetization.

The presence of retained austenite simultaneously increases the coercive force and decreases the saturation magnetization and mechanical hardness.

The reverted austenite reduces the intensity of the {111} fiber in the martensite phase.

The reverted austenite carries a crystallographic texture similar to that seen in FCC alloys with Goss and copper components.

EBSD studies compared with calculated orientations using the phenomenological theory of martensite suggest that both the reverted and the parent austenites have the same crystallographic texture, thus indicating that a texture memory effect was active during the transformation.

References

[1] E.V. Belozerov, V.V. Sagardaze, A.G. Popov, A.M. Pastukha, N.L. Pecherkina, Formation of magnetic texture in a high-strength maraging steel, Phys. Met. Metallogr. 79 (6) (1995) 606.
[2] A. Magnée, J.M. Drapier, J. Dumont, D. Coutsouradis, L. Habraken, Cobalt Containing High Strength Steels, Centre d'Information du Cobalt, Brussels (1974), p. 128.
[3] M. Ahmed, K. Hasnain, I. Nasim, H. Ayubh, Magnetic properties of maraging steel in relation to deformation and structural phase transformations, Acta Metall. Mater. 42 (3) (1994) 631.
[4] S.S.M. Tavares, H.F.G. Abreu, J.M. Neto, M.R. Silva, I. Popa, A magnetic study of the maraging 350 Steel, J. Magn. Magn. Mater. 272 (2004) 785.
[5] D.T. Peters, Source Book on Maraging Steels, ASM, Materials Park, Ohio (1979), p. 304.
[6] M. Farooque, H. Ayub, A.U. Haq, A.Q. Khan, The formation of reverted austenite in 18% Ni 350 grade maraging steel, J. Mater. Sci. 33 (1998) 2927.
[7] S.S.M. Tavares, H.F.G. Abreu, J.M. Neto, M.R. Silva, I. Popa, A thermomagnetic study of the martensite–austenite phase transition in the maraging 350 steel, J. Alloy. Compd. 358 (2003) 152.
[8] M. Ahmed, A. Ali, S.K. Hasnain, H. Hashmi, A.Q. Khan, Magnetic properties of maraging steel in relation to deformation and structural phase transformation, Acta Metall. Mater. 42 (3) (1994) 631.
[9] L. Xiaodong, Y. Zhongda, Reverted austenite during aging in 18Ni(350) maraging steel, Mater. Lett. 24 (4) (1995) 239.
[10] J.M. Pardal, S.S.M. Tavares, M.C. Fonseca, H.F.G. Abreu, J.J.M. Silva, Study of the austenite quantification by X-ray diffraction in the 18Ni–Co–Mo–Ti maraging 300 steel, J. Mater. Sci. 41 (8) (2006) 2301.
[11] N. Nakada, T. Tsuchiyama, S. Takaki, S. Hashizume, Variant selection of reverted austenite in lath martensite, ISIJ Int. 47 (10) (2007) 1527.
[12] S. Kundu, H.K.D.K. Bhadeshia, Crystallographic texture and intervening transformations, Scr. Mater. 57 (2007) 869.
[13] S. Kundu, H.K.D.K. Bhadeshia, Transformation texture in deformed stainless steel, Scr. Mater. 55 (2006) 779.
[14] J.S. Bowles, J.K. MacKenzie, The crystallography of martensite transformations I, Acta Metall. 2 (1954) 129.
[15] J.K. MacKenzie, J.S. Bowles, The crystallography of martensite transformations II, Acta Metall. 2 (1954) 138.
[16] H.K.D.K. Bhadeshia, Geometry of Crystals, 2nd edition,. Institute of Materials, London, 2001.
[17] K.W. Andrews, Empirical formulae for the calculation of some transformation temperatures, J. Iron Steel Inst. 203 (1965) 721.
[18] W. Sha, Z. Guo, Maraging Steels Modelling of Microstructure, Properties and Applications, Woodhead Publishing Limited, United Kingdom, 2009.
[19] M. Farooq, A.U. Haaq, F.H. Hashmi, A.Q. Khan, Microscope determination of austenite in 18% Ni maraging steel, Metallography 20 (1987) 377.
[20] H.G. Bowden, P.M. Kelly, The crystallography of the pressure induced phase transformations in iron alloys, Acta Metall. 15 (1967) 1489.